Atmospheric Research 266 (2022) 105972

Contents lists available at ScienceDirect

Atmospheric Research

journal homepage: www.elsevier.com/locate/atmosres

Numerical simulation of the microphysics and liquid chemical processes occur in fog using size resolving bin scheme

Jeevan Kumar Bodaballa [a,*], Istvan Geresdi [a], Sachin D. Ghude [b], Imre Salma [c]

[a] University of Pécs, Faculty of Sciences, Pécs, Hungary
[b] Indian Institute of Tropical Meteorology, Pune, India
[c] Eötvös Loránd University, Faculty of Science, Budapest, Hungary

ARTICLE INFO

Keywords:
Fog microphysics
Liquid-phase chemistry
Scavenging
Air pollution
Aerosol regeneration

ABSTRACT

This research aims to understand the role of the initial hygroscopicity of aerosol particles, scavenging mechanisms and of aqueous chemistry in the evolution of the aerosol size distribution. A box model with a size resolving moving bin scheme is used to simulate the fog events over Budapest (Hungary) and Delhi (India). The results from the study are as follows: (i) Aerosol particles can be washed out from the atmosphere more efficiently by Brownian and phoretic scavenging than by activation processes. The efficiency of scavenging mechanisms depends on the size distribution of the dry aerosol particles and the size dependence of the hygroscopicity of the aerosol particles. The efficiency of the phoretic scavenging is also impacted by the duration of the dissipation phase of the fog. (ii) The liquid-phase chemistry, which occurs inside the droplets due to their long residence times in the atmosphere, significantly impacts the size distribution of the regenerated particles. (iii) The liquid-phase chemistry also impacts the hygroscopicity of the regenerated aerosol particles. The enhancement of the concentrations of NH_4^+, NO_3^- and $S(VI)$ ions inside the droplets result in a substantial increase of the hygroscopicity of the water-soluble particles. This higher hygroscopicity may impact the fog dissipation by increasing the solution effect and helps to uphold successive fog events under favorable environmental condition.

1. Introduction

Fog is a persistent meteorological phenomenon in the wintertime over metropolitan areas. It leads to monetary losses such as flight delays and accidents, resulting in an increment in the death rate. The fog consists of suspended water droplets or ice crystals near the Earth's surface that forces a devaluation of horizontal visibility below 1 km (Gultepe et al., 2007b). Fog forms, strengthens, and disperses as a result of complex interactions among diverse local, microphysical, dynamical, radiative, and chemical processes, along with boundary layer conditions (Gultepe et al., 2007b). Aerosol particles play a vital role in fog formation, development, and dissipation. Furthermore, the fog can also impact the characteristics (e.g. size distribution, chemical composition) of the aerosol particles. The main sources of particle numbers in cities are traffic, construction, thermal power stations, factories and household emissions, and their concentration is affected by advection and scavenging processes. While scavenging by activation strongly depends on the chemical composition of the particles (e.g., Gilardoni et al., 2014), the collision mostly scavenges particles affected in size by water drops. A number of observation and numerical models have proven that generally, the nucleation of hygroscopic particles is the dominant scavenging mechanism in the washout of the water-soluble particles (Steinfeld, 1998; Elbert et al., 2000; Gilardoni et al., 2014). However, this is not necessarily happening in fog, where the supersaturation is low (generally <0.05%), and as a consequence, only a small percentage (< 10%) of the water-soluble particles are activated (Boutle et al., 2018; Gilardoni et al., 2014). The aerosol particles (both hydrophobic and hygroscopic) smaller than 0.1 μm can remain in the interstitial space or can be scavenged by small drops in the fog. Izhar et al., 2020 collected aerosol and fog water samples over the Indo Gangetic Plain. They found that aerosol concentration reduced during fog periods compared to non-fog periods, due to scavenging by fog droplets. Furthermore, Kunkel, 1982 explained haze particles as wet aerosol particles with low hygroscopicity that are not yet activated to form drops. Most activated particles remain in the atmosphere after the dissipation of the fog, since small fog drops and haze particles do not sediment. Recent numerical weather prediction model (NWP) sensitivity tests explained that in a well-mixed fog, an increase in aerosol concentrations (as long as saturate

* Corresponding author.
E-mail address: jeevan@gamma.ttk.pte.hu (J.K. Bodaballa).

https://doi.org/10.1016/j.atmosres.2021.105972
Received 6 August 2021; Received in revised form 6 December 2021; Accepted 12 December 2021
Available online 15 December 2021

or near saturated) would enable the formation optically thick fog, and to persist for extended time intervals by increasing droplet concentration (Boutle et al., 2018). Wang et al., 2014 asserted that in a metropolitan area, more-hygroscopic-mode particles were made of aged background particles and that less-hygroscopic-mode particles contained high amounts of soot (elemental carbon, EC) and carbonaceous compounds, dust particles, and high-mass organic particles. Nevertheless, the association of particles that have different hygroscopicity with chemical composition, origin, and formation processes of particles has still been missing.

The chemical composition and the size distribution of aerosol particles are affected not only by their sources, along with gas-phase chemical reactions and microphysical processes but also by the chemical reactions that occur in the water drops. Dissolution of some ambient gases into droplets and the subsequent aqueous-phase chemical reactions can also modify the particle size (Kerminen and Wexler, 1995; Meng and Seinfeld, 1994). For the previous few decades, understanding and predicting the near surface weather phenomena have been among the greatest challenges. However, researchers followed some actual cases and even forecasted them successfully. Nevertheless, forecasting fog events are challenging due to the lack of detailed knowledge and investigations. Moreover, the numerical weather forecast models are also inadequate to anticipate the specific location and time evolution of the fog period (Mazoyer et al., 2019). Cui et al., 2019, compared the validated simulations of weather research forecast (WRF) model with WRF nested Large Eddy Simulation (WRF-LES) model. They proved that WRF-LES simulated the various physical parameterizations at near surface significantly better. They also asserted that results of WRF simulations were highly sensitive to various physical parametrization schemes (e.g., Chaouch et al., 2017). Besides, considering the chemistry in fog models is the greatest challenge due to a lack of observational data of trace gases and various relevant inorganic and organic compounds for validating the models.

Bott et al., 1990 used a 2D bin microphysical scheme to describe the nucleation scavenging. This scheme simulates both the formation and diffusional growth of water drops rather accurately. However, the application of this scheme is computationally too expensive even nowadays, and it was used only in 1D simplification. Although the box models are not able to simulate some important characteristics of the fog (e.g. turbulence, radiative cooling, sedimentation), they allow for the very accurate simulation of specified processes such as microphysical and chemical processes. For example, Xue et al., 2019 carried out box model experiments using bulk liquid chemistry scheme that incorporated detailed SO_2 oxidation chemistry to derive SO_4^{2-} production over the full range of SO_2 atmospheric concentrations.

Budapest and Delhi are the capital cities of Hungary and India. The cities have different characteristics based on population density, traffic, industrialization, and agricultural activities. We have taken two observed fog events from both cities and simulated them to understand their microphysical characteristics. In this study, we compare fog microphysical characteristics of a city center (Budapest, Hungary) and an industrial area (airport, Delhi). The main aims of this research are:

- to understand and discuss the impact of the characteristics of aerosol particles on the formation and dissipation of fog,
- to reveal and quantify the scavenging processes of sub-micron particles,
- to study and interpret the regeneration of aerosol particles through the chemical process in the fog.

2. Model description

A detailed bin scheme with moving boundaries was used to simulate the diffusional growth or evaporation of water drops as published by Geresdi and Rasmussen, 2005. The model involves 28 bin categories in the Budapest case and 95 bins in the Delhi case (the number of the bins depends on the size resolution of the observation) for both the hygroscopic and hydrophobic particles, and initially, the whole spectrum of bins extends from the mass of 1.22×10^{-22} to 1.02×10^{-15} kg from radius of 0.005 μm to radius of 0.7 μm) and from 5.55×10^{-22} to 1.59×10^{-17} kg (from radius of 0.0042 μm to radius of 0.12 μm), respectively. The water drops and the haze particles were allowed to form on the hygroscopic particles, the hydrophobic particles were supposed to remain dry. The evolution of the haze particle and water droplet size distributions due to the diffusional growth, and the changing of the aerosol composition via chemical processes were calculated at each bin. The fog formation was simulated using a box model due to the fact that the solution of the stiff, ordinary differential equation system describing the chemical processes is computationally rather expensive. Some dynamical processes (e.g. turbulent mixing, the radiation effect at the top of the fog and the sedimentation of the water drops), which could be important in the evolution of the fog, were not taken into consideration since we focused on fog microphysics and the interaction between the microphysics and chemistry in this approach. The fog formation is simulated by holding the water content (sum of vapor and liquid) to be constant and decreasing the temperature gradually. The cooling rate and warming rate is tuned to fit the time profile of the simulated temperature to the observed one. The formation of haze particles is initiated as the saturation ratio reaches the value of 95%. The initial mass of the haze particles is supposed to be double the mass of the aerosol particles they formed on. Further change of the mass of haze particles/water drops is calculated by the integration of the following equation based on Pruppacher and Klett, 2010:

$$\frac{dm_d}{dt} = 2\pi D_d \frac{\left[S - 1 - \frac{4\sigma w_a}{R_v T \rho_w D_d} + \frac{\varepsilon \upsilon M_w m_p}{M_s\left(m_d - m_p\right)}\right] f_v}{\frac{L_v}{k_a^* T}\left[\frac{L_v}{R_v T} - 1\right] + \frac{R_v T}{e_{sat,w} D_v^*}} = 2\pi D_d \frac{\left[S - 1 - \frac{4\sigma w_a}{R_v T \rho_w D_d} + \kappa \frac{\rho_w m_p}{\rho_p\left(m_d - m_p\right)}\right] f_v}{\frac{L_v}{k_a^* T}\left[\frac{L_v}{R_v T} - 1\right] + \frac{R_v T}{e_{sat,w} D_v^*}} \quad (1)$$

where m_d and D_d are the mass and the diameter of water drops (sum of liquid water mass and aerosol mass), respectively; m_p and ρ_p are the mass and the density of dry aerosol particles the drop formed on, respectively; M_w and M_s are the molecular weight of water and the compounds the aerosol particles are composed of, respectively. ε and ν are the water-soluble fractions of the aerosol particles and the van't Hoff factor, respectively. S, T, k_a* and D_v* are saturation ratio, temperature, the thermal conductivity of air, and the diffusivity of vapor in the air, respectively. L_v, R_v, $e_{sat,\,w}$, σ are the latent heat of condensation, specific gas constant for water vapor, saturated vapor pressure over liquid water surface at ambient temperature, surface tension, respectively. The κ hygroscopicity parameter depends on the chemical composition of aerosol particles. The correction due to the kinetic effect is taken into consideration in the case of thermal conductivity and diffusivity (Pruppacher and Klett, 2010). The equation above is solved in parallel with the droplet formation on particles with different diameters and hygroscopic properties.

The radiative cooling causes the cooling of the airmass, and the saturation is simulated by reducing the temperature at prescribed rates. In simple terms, the fog evolution is mimicked by a prescribed cooling and warming rate based on the time evolution of the observed temperature. The impact of the latent heat of condensation and evaporation is taken into consideration for the prescription of the cooling and warming rate.

The visibility is calculated as per the following equation (Silverman et al., 1974):

$$V = \frac{3.912}{\pi \sum_{i=1}^{n} K_i N_i r_i^2} \quad (2)$$

where N_i, r_i are the concentration and radius of droplets in the i^{th} particle size category, respectively. κ_i is the scattering efficiency for the droplets, with a value of 2 regardless of the drop size. The size dependence of the extinction coefficient can be significant if the drop radius is less than 3 μm (e.g., Gultepe et al., 2006; Song et al., 2019). However, our sensitivity study proves that neglecting the size dependence of the extinction coefficient results in a false visibility value only in the case of haze. If the fog consists of drops larger than a few microns, the impact of the haze particles on the visibility is small.

The numerical model involves the following processes:

- The liquid water content in each bin is evaluated by solving the Eq 1. The integration is performed in a time step of 0.0001 s. This small time step allows us to avoid the overestimation of the diffusional growth in the case of small drops when the solution is dense. Furthermore, the competition for available vapor among drops with different sizes and with a different type and size of aerosol particles inside them can be taken correctly into consideration.
- The scavenging of aerosol particles ($r < 1.0$ μm) by water drops through Brownian motion and phoretic forces.Theory published by Pruppacher and Klett, 2010 is used to evaluate the impact of Brownian and phoretic impaction scavenging. While Brownian scavenging is efficient if the particle size is less than 0.1 μm, phoretic scavenging can reduce the concentration of the particles with a radius of about 0.1 μm (Santachiara et al., 2013). The latter process persists only in a subsaturated environment so that it can happen during either the formation or dissipation of the fog. In this study, we focus on the scavenging efficiency of Brownian motion and phoretic force. The impacts of gravitational collection and turbulence are not taken into consideration. The scavenging of particles with a radius less than 1 μm, both hydrophobic particles and haze, due to the Brownian motion and phoretic scavenging are calculated separately.
- The absorption and desorption of the trace gases of SO_2, NH_3, H_2O_2, HNO_3, O_3 and CO_2. Sulphate formation in the liquid phase due to oxidation of $S(IV)$ by O_3 and H_2O_2. The amount of the dissolved trace gases and that of sulfate formed due to the chemical reaction were evaluated for each bin with a droplet radius larger than 1 μm. The stiff, ordinary differential equations about the chemical processes are solved by using time step of 0.0001 s.

3. Data and methods

For the Budapest case, the size distribution and hygroscopicity of the aerosol particles were obtained in a field project at the Budapest platform for Aerosol Research and Training (BpART) Lab (Salma et al., 2016) in Budapest (47.474°N,19.062°E) from 9 December 2014 to 9 February 2015 (Enroth et al., 2018). The observational setup was located at 114 m above mean sea level, an 85 m distance from the river Danube, and at a height of 12–13 m from street level. More details about the experiments can be found elsewhere (Enroth et al., 2018). The focus of this research was not on fog, so data about visibility is not available. However, both the temperature and relative humidity of the ambient air was recorded. It is supposed that fog is formed if the observed relative humidity is equal to or larger than 99%, for longer than 1 h. Based on this data, 14 fog periods could be defined in the observational period. The Hungarian Meteorological Service (hereafter HMS) also confirmed these fog events in the Budapest region. The fog event which occurred from 31 January 2015 to 01 February 2015 was chosen for this study. The presence and the duration of the fog were confirmed by low wind speed ($<1\ ms^{-1}$), street cameras, and it was also detected by HMS at the

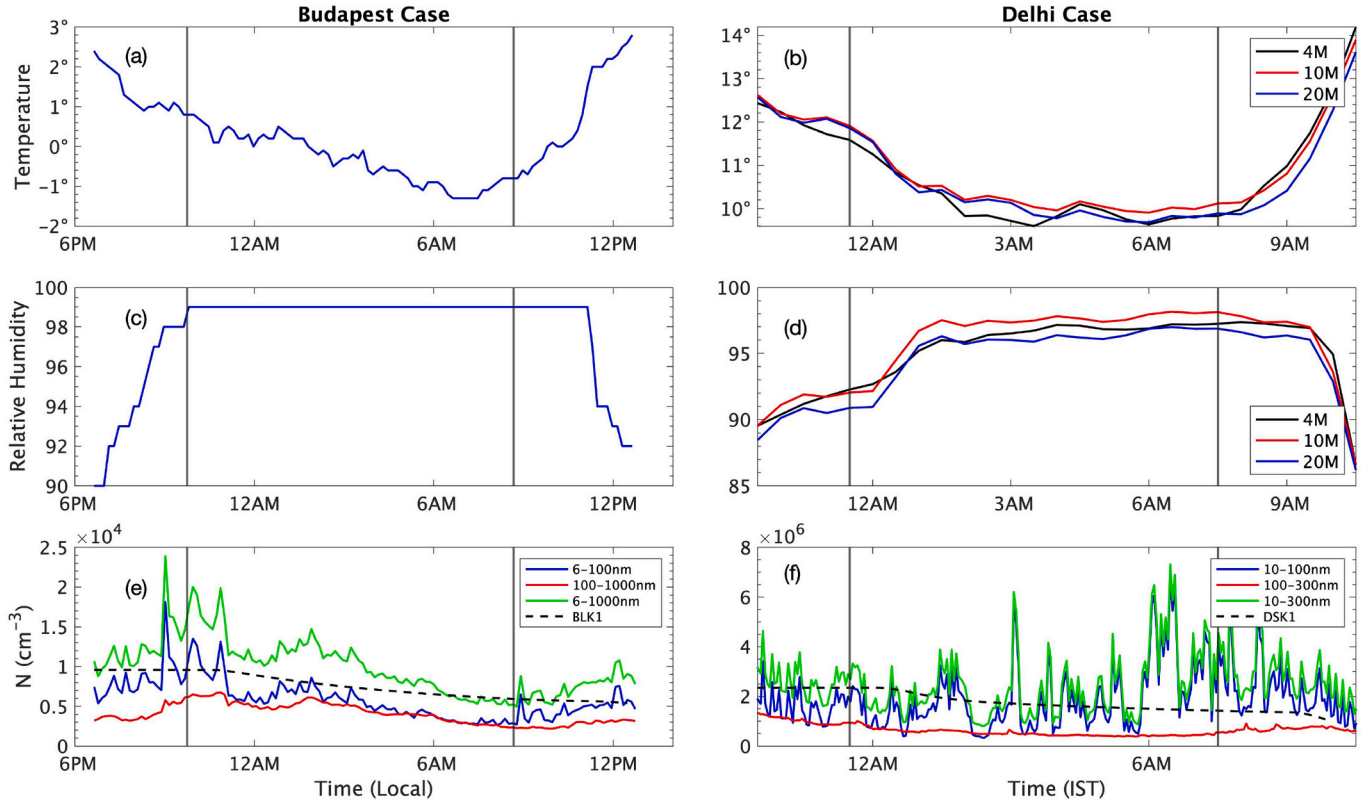

Fig. 1. Observed temperature (a) and (b), relative humidity (c) and (d), furthermore the observed number concentration of aerosol particles in different size ranges (e) and (f). The lines with different colors in panel (b) and (d) denote the data belong to different elevation of the observation from the surface. The dashed line in the panel (e) and (f) shows the time profile of the simulated number concentrations. Vertical lines denote the start and the end of the fog.

South–East region of Budapest. Fig. 1 shows the temporal variability of the fog onset, offset, T, RH, and number concentration (N) of ultrafine (6–100 nm), chemically aged (100–1000 nm), and total particles (6–1000 nm).

In order to better understand the changes of the characteristics of aerosol particles in the fog, we simulate the impact of trace gases. Concentrations of SO_2, NH_3, HNO_3, O_3 provided by HMS are used to give the trace gas concentration in the atmosphere for the Budapest case. The daily average trace gas concentrations are available for NH_3, and HNO_3 so we consider these as initial values. Furthermore, the concentration of these trace gases in the atmosphere is not allowed to reduce under one-tenth of the initial concentration (Table 1). This means that we suppose the trace gases are partly supplied by advection or local sources. In the case of SO_2 and O_3, the hourly measured data shows that their concentrations were nearly constant during the fog event. In this SO_2 case, we make a sensitivity test to study how the concentration impacts the chemical processes occurring in the fog droplets: (i) the SO_2 concentration is held constant as it was observed, (ii) the SO_2 concentration is allowed to reduce, but not below one tenth of the initial concentration due to the absorption. The unique aspect of the Budapest data for the aerosol particles is that it involves information about the size dependence of the hygroscopicity (Enroth et al., 2018). The hygroscopic properties were derived by a Volatility-Hygroscopicity Tandem Differential Mobility Analyzer (VH-TDMA) measurement system. Less-hygroscopic (LH) and nearly-hydrophobic (NH) particles are separated, based on the measurements of the hygroscopic growth factors (HGFs) at different dry diameters of 50, 70, 110 and 145 nm. The number fraction of nearly hydrophobic particles, based on this observation, is plotted in Fig. 2. On the observation data, linear and power function trend lines are fitted to make the distinction between LH and NH particles at the diameter ranges (Fig. 2). The vapor uptake by both types of particles is calculated by integrating Eq. 1. To study the sensitivity of fog formation in terms of the size dependence of the hygroscopicity, a mean hygroscopicity would characterize all the aerosol particles evaluated in the Budapest case:

$$\kappa_{mean} = \sum_{i=1}^{n} \frac{V_{1,i}N_{1,i}\kappa_{LH} + V_{2,i}N_{2,i}\kappa_{NH}}{V_{1,i}N_{1,i} + V_{2,i}N_{2,i}} \quad (3)$$

where n is the number of bins, $V_{1,\,i}$, $V_{2,\,i}$ are volumes of LH and NH particles in the i^{th} bin, respectively, $N_{1,\,i}$, $N_{2,\,i}$ are the number concentrations of the LH and NH categories at the i^{th} bin. κ_{LH} and κ_{NH} are measured hygroscopicity parameters of less-hygroscopic and nearly-hydrophobic particles (κ=0.2 and 0.03), respectively.

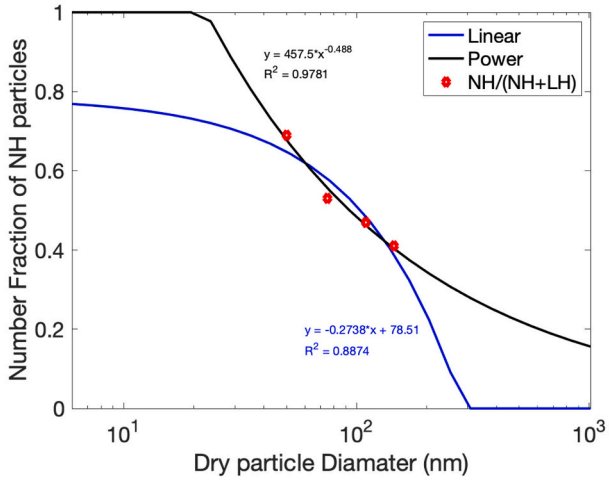

Fig. 2. Fitted linear and power functions to give the fraction of NH particles for the whole spectrum. The red dotes denote the observed fractions. (Note: LH and NH denotes less hygroscopic and nearly hydrophobic dry aerosol particles).

The air pollution in the Delhi case was larger. The observational site was located at Indira Gandhi International Airport (IGIA, 28.56°*N*,77.09°*E*), Delhi, India. This is one of the biggest airports in the world and it is about 240 m above mean sea level. In the current research, we use the data observed in intensive observational periods during winter fog experiments (WIFEX; Ghude et al., 2017). During this experimental campaign, a micro-meteorological tower with a height of 20 m was set up at the site, which measured the boundary layer characteristics such as T and RH at different levels. For our model simulation, data are considered from the 10 m height level and the average surface visibility was reported to be about 100 m (Pithani et al., 2020). Scanning mobility particle sizer (SMPS) was used to measure the number size distribution of dry aerosol particles in a diameter range of 10–300 nm (Ghude et al., 2017; Pithani et al., 2020). Trace gas concentrations of SO_2, NH_3, HNO_3 measured and published by Acharja et al., 2020 for the same location but a different fog event are given as initial conditions, due to the lack of available trace gas concentration data at 30 December 2016. The temporal evolution of the gas concentration is treated the same way as in the Budapest case. For our model simulation, one fog event (started at 30 December 2016, 23:30 LT (18:00 UTC) – dissipated

Table 1
Initial conditions with different hygroscopicity parameter (κ) and different gas concentrations (kg/kg) for Budapest and Delhi cases along with sensitivity test ID. (Note: SO_2 concentration with * means constant SO_2 source throughout the simulation.)

Case	Category	Test ID	SO_2 (kg/kg)	HNO_3 (kg/kg)	NH_3 (kg/kg)	H_2O_2 (kg/kg)	O_3 (kg/kg)
	Linear function (κ_{LH} = 0.2, κ_{NH} = 0.03)	BLK1	*6.4×10^{-9}	4.2×10^{-11}	4.5×10^{-10}	1.1×10^{-10}	4.8×10^{-9}
		BLK2	*6.4×10^{-9}	0	4.5×10^{-10}	1.1×10^{-10}	4.8×10^{-9}
		BLK3	6.4×10^{-9}	4.2×10^{-11}	4.5×10^{-10}	1.1×10^{-10}	4.8×10^{-9}
		BLK4	6.4×10^{-9}	0	4.5×10^{-10}	1.1×10^{-10}	4.8×10^{-9}
Budapest Case	Power function (κ_{LH} = 0.2, κ_{NH} = 0.03)	BPK1	*6.4×10^{-9}	4.2×10^{-11}	4.5×10^{-10}	1.1×10^{-10}	4.8×10^{-9}
		BPK2	*6.4×10^{-9}	0	4.5×10^{-10}	1.1×10^{-10}	4.8×10^{-9}
		BPK3	6.4×10^{-9}	4.2×10^{-11}	4.5×10^{-10}	1.1×10^{-10}	4.8×10^{-9}
		BPK4	6.4×10^{-9}	0	4.5×10^{-10}	1.1×10^{-10}	4.8×10^{-9}
	homogenous hygroscopicity (κ_{mean} = 0.145)	BMK1	*6.4×10^{-9}	4.2×10^{-11}	4.5×10^{-10}	1.1×10^{-10}	4.8×10^{-9}
		BMK2	*6.4×10^{-9}	0	4.5×10^{-10}	1.1×10^{-10}	4.8×10^{-9}
		BMK3	6.4×10^{-9}	4.2×10^{-11}	4.5×10^{-10}	1.1×10^{-10}	4.8×10^{-9}
		BMK4	6.4×10^{-9}	0	4.5×10^{-10}	1.1×10^{-10}	4.8×10^{-9}
Delhi case	κ_{LH} = 0.42, κ_{NH} = 0.03	DSK1	*1.78×10^{-8}	2.2×10^{-10}	2×10^{-8}	1.1×10^{-9}	3.3×10^{-8}
		DSK2	*1.78×10^{-8}	0	2×10^{-8}	1.1×10^{-9}	3.3×10^{-8}
		DSK3	1.78×10^{-8}	2.2×10^{-10}	2×10^{-8}	1.1×10^{-9}	3.3×10^{-8}
		DSK4	1.78×10^{-8}	0	2×10^{-8}	1.1×10^{-9}	3.3×10^{-8}
	homogenous hygroscopicity (κ_{mean} = 0.3)	DMK1	*1.78×10^{-8}	2.2×10^{-10}	2×10^{-8}	1.1×10^{-9}	3.3×10^{-8}
		DMK2	*1.78×10^{-8}	0	2×10^{-8}	1.1×10^{-9}	3.3×10^{-8}
		DMK3	1.78×10^{-8}	2.2×10^{-10}	2×10^{-8}	1.1×10^{-9}	3.3×10^{-8}
		DMK4	1.78×10^{-8}	0	2×10^{-8}	1.1×10^{-9}	3.3×10^{-8}

at 31 December 2016, 07:30 LT (02:00 UTC)) is taken into consideration and sensitivity tests are made with different κ values and trace gas concentrations. Because bulk hygroscopicity parameters were measured in Delhi during the Delhi Aerosol Supersite (DAS) campaign, there is no available information about the size dependence of the κ value in this case. The average hygroscopicity parameter is evaluated from the observed data by using the mixing rule (Petters and Kreidenweis, 2007), which resulted in approximately 0.3 (Arub et al., 2020). Pringle et al., 2010 simulated the global (land mass) mean κ value and SD and obtained 0.27±0.21, which is in line with our estimated and adopted κ value. The sensitivity on the size dependence of the hygroscopicity is studied by separate simulations:

The hygroscopicity of all aerosol particles is the same as the value available from the field project.

The aerosol particles for the Delhi case are hypothetically divided into two categories. All the particles less than 130 nm in diameter are supposed to be NH particles and their κ value is supposed to be equal to 0.03. There is observation data which support that choosing this diameter to separate the hygroscopic and hydrophobic particles is reasonable. Plots in Fig. 2 show that more than 60–70% of the particles are found to be hygroscopic in Budapest downtown if the particle diameter is larger than 130 nm. On the bases observations in China, Wang et al., 2018 asserted that dry aerosol particles with a diameter of 200 nm had a significantly larger hygroscopic growth factor compared to particles with a diameter of 50 nm. Using these assumptions and substituting the average κ value (0.3) into the left-hand side of the Eq. 3. the value of the κ value for the LH particles can be evaluated. In this case the evaluated κ value of LH particles larger than 130 nm is 0.42.

The initial conditions for the numerical simulation are the size distribution of the aerosol particles before the onset of fog over Budapest and Delhi plotted in Fig. 3a, and 3c, as well as in Fig. 3b and 3d, respectively. The initial aerosol size distributions shown in Fig. 3c and 3d represent the cases when the aerosol particles are divided into categories of LH and NH. For a better understanding of fog chemistry, we performed several sensitivity tests with different hygroscopicity, and different environmental conditions (trace gas concentrations) summarized in Table 1 along with test ID.

4. Results

4.1. Time profiles of the fog evolution

Fig. 4 shows the time profiles of simulated and observed fog events. Also, the fog onset, mature period and dissipation for both the Budapest and Delhi cases are indicated. In the Budapest case, the fog onset and dissipation were based on the observed RH ≥99% and street camera visibility. Our model shows a 1-h delay of fog onset in the Delhi case, but in the Budapest case fog onset is simulated well. However, the time of dissipation in both the Budapest and Delhi cases is delayed by 2–3 h. These discrepancies can be the consequence of the fact that in our box model only the impact of the cooling/warming is taken into consideration, and the effect of any other processes (e.g., turbulent mixing, sedimentation) neglected. Fig. 4a and 4b show the observed and simulated time profiles of temperature and relative humidity of the Budapest and Delhi cases. The fitting of the temperature profiles in both cases shows how well the observed temperature profile is reproduced by prescribed cooling and warming rates (Note: the temperature is affected by both the radiative cooling rate and the releasing latent heat of

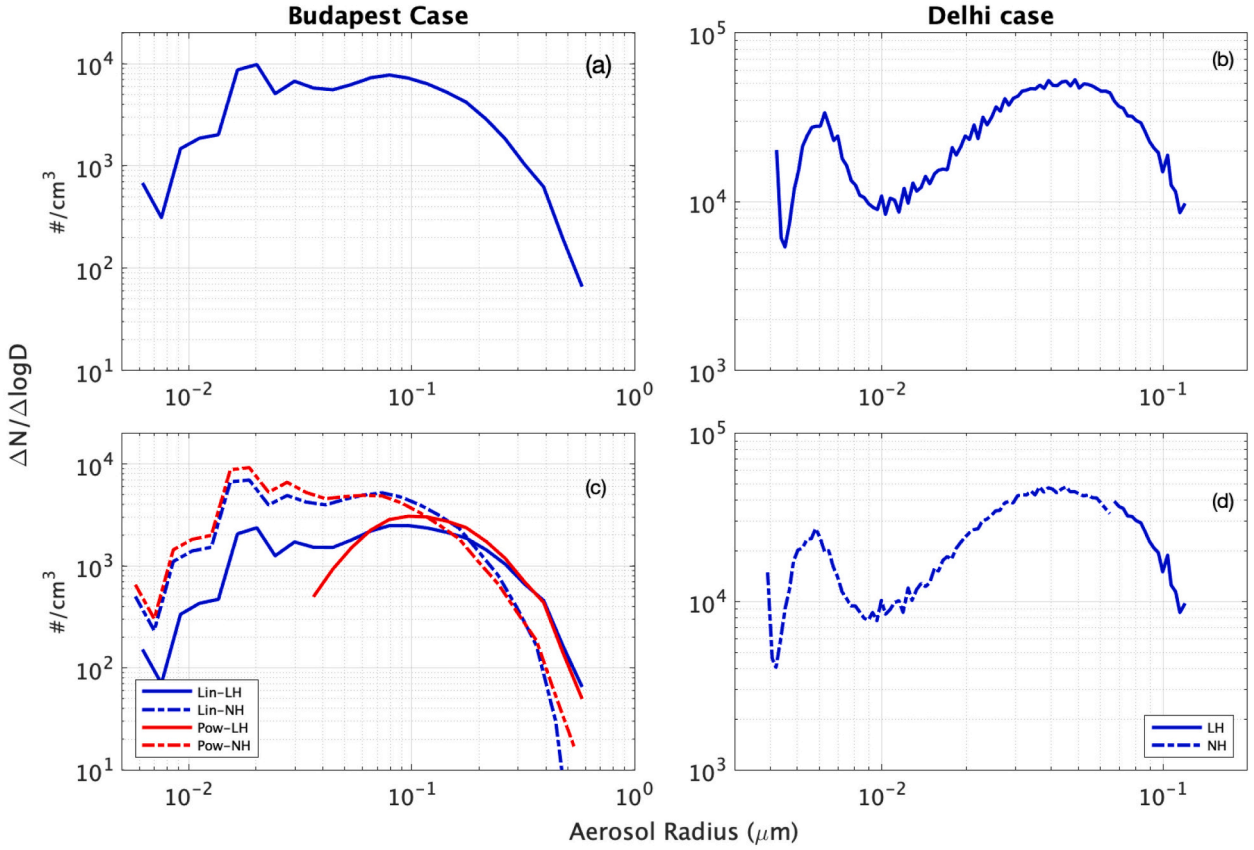

Fig. 3. Initial size distribution of particles of observed and model input over Budapest and Delhi fog events. Observed dry aerosol size distributions are plotted in panel (a) and (b). Panel (c) and (d) reveal the distinction of aerosol particles into the categories of less hygroscopic (LH) and near hydrophobic (NH) over BLK1 and DSK1. Size distributions plotted in panel (a) and (b) are used if the size dependence of the κ value is neglected. The legend in panel c denotes the way of the separation of LH and NH particles.

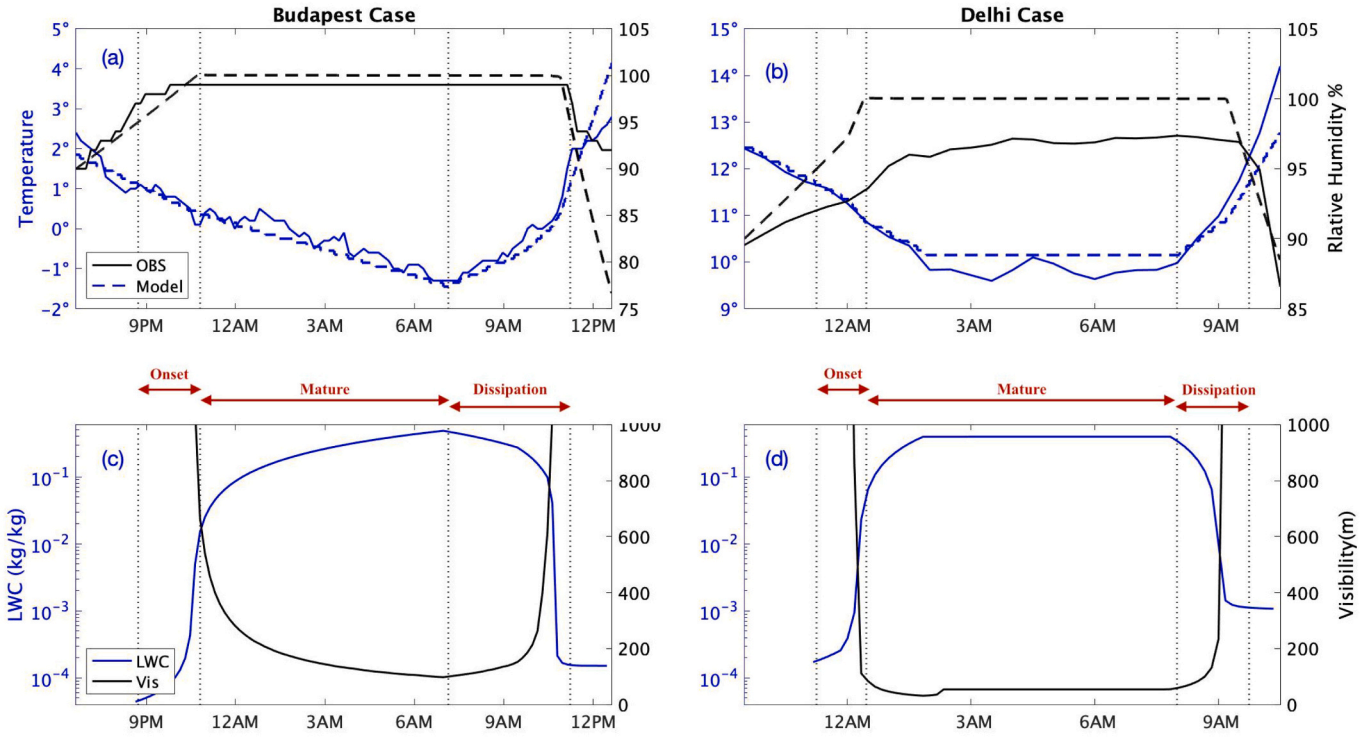

Fig. 4. Evolution fog over Budapest (at 31 January 2015–1 February 2015) and Delhi (30–31 December 2016). Panel (a) and (b): Observational and model data of temperature and RH for Budapest and Delhi cases. Panel (c) and (d): Simulated LWC and visibility for both Budapest and Delhi cases. The vertical dashed lines indicate the evolution periods of the fog.

condensation). The difference between the simulated and observed time profiles of the relative humidity is more significant, mostly in the Delhi case. However, this discrepancy can be explained by measurement error. Generally, the RH sensors measure up to 95%, and they usually do not reach 100% (Gultepe, 2019; Gultepe et al., 2007a).

Based on the time evolution of the liquid water content, we define three phases in the life cycle of the fog (Fig. 4c, 4d). The period when the LWC increases significantly before the supersaturation reaches its maximum value is called the onset period of the fog (LWC hereafter means the sum of the liquid water mixing ratios calculated in each bin, and as such in our model output the LWC includes the haze particles as well, however the mixing ratio of the haze particles is about one-two order lesser than that of the fog droplets). The next period remains until the supersaturation drops below 0, this period is called the mature fog phase. The last phase is when the drops start to evaporate, which is called the dissipation period. These periods are indicated by vertical dashed lines in Fig. 4. At the time when visibility drops below 200 m, the value of LWC is 0.00013 kg/kg (near 0.13 gm^{-3}) and 0.00008 kg/kg (near 0.08 gm^{-3}) in the Budapest and Delhi case, respectively. The larger concentration of haze particles and water drops in the Delhi case explains why the dense fog can form in Delhi even at a smaller LWC. Unfortunately, no observed LWC data is available to verify our calculated data. The formula suggested by Gultepe et al., 2006 can be used to estimate LWC if the visibility and concentration of the fog drops are known. Since the reported visibility Pithani et al., 2020 is between 50 and 100 m and the number concentration of the fog drops is about 250 cm^{-3} (see the concentration of the activated aerosol particles in Table 2), the LWC should be between 0.41 and 0.14 gm^{-3}. During the WIFEX campaign, the evolution of the fog events in Delhi was simulated by WRF mesoscale model (Pithani et al., 2020) and presented the LWC about 0.2 gm^{-3} at the middle phase of the fog development. However, in our current simulation the LWC is about 0.4 gm^{-3} in the mature phase of the fog for the same case. The discrepancy between these two values can be explained by different model configurations (e.g., the turbulent mixing and sedimentation is not considered in our model simulation). The dissipation rate of the fog depends mostly on the warming rate. The LWC starts to decrease when the saturation drops below 100% at about 7:00 am in the Budapest case and at about 8 am in the Delhi case. The LWC decreases only slightly between 7 am and 11 am in Budapest, because of the small warming rate (about 0.3°Ch^{-1}) in this time period. Later, the warming rate becomes significantly larger (about 1.5°Ch^{-1}), and the fog dissipates very fast, within 30 min. In the Delhi case, the average warming rate is about 1°Ch^{-1} which results in different dissipation pattern comparing to the Budapest case. As a consequence of the different warming rates, it takes more than 90 min and less than 60 min to drop the relative humidity from near 100% to 90% in the Delhi and Budapest cases, respectively.

4.2. *The impact of the scavenging*

Scavenging of small aerosol particles by water drops is a self-cleaning mechanism in the atmosphere. Due to the very small supersaturation (of 0.0004 and 0.0007 in the Budapest and Delhi cases respectively, shown as s_{max} in the second column of Table 2), the activation reduces the number concentration of even the hygroscopic particles in fog only slightly. Fig. 5 summarizes the results of the numerical simulation about the efficiency of the different scavenging mechanisms. Fig. 5a and 5b show the temporal evolution of the accumulated numbers of scavenged particles in the BLK1 and BMK1, as well as in the DSK1 and DMK1 cases (these cases provide a good representation well of all the simulated cases if only scavenging is considered). Fig. 5c reveals that the liquid chemical processes have no impact on the scavenging processes in either the Budapest or the Delhi cases (See case ID in Table 1). In both cases, the temporal variation of the scavenging rates is related to temporal variation of the LWC. While the impact of the Brownian motion is dominant in all of the investigated cases, the role of the phoretic scavenging mechanism is negligible in the Budapest cases and is more significant in the Delhi cases (Fig. 5c and Table 2). In the Budapest cases, the results do

Table 2
Summary of maximum supersaturation (s_{max}), critical radius of droplet (r_{cd}) for the hygroscopic particles, total activated aerosols at s_{max}, maximum LWC, initial number concentration of the aerosol particles (N), scavenging and relative effect of Brownian and phoretic scavenging and total amount of scavenged particles during the period when RH>95%, change of maximum aerosol size (Δr_{aer}) by the end of the dissipation period.

Test ID	s_{max}	r_{cd} (μm)	Activated aerosol ($\#/cm^3$)	LWC_{max} (gm^{-3})	N ($\#/cm^3$)	N_{Br} ($\#/cm^3$)	N_{Br}/N	N_{ph} ($\#/cm^3$)	N_{ph}/N	Total scavenged %	Δr_{aer} (μm)
BLK1	4.61×10^{-4}	1.74	50	0.487	8500	3290	38.84%	86	1.02%	39.86%	0.45
BLK2	4.61×10^{-4}	1.74	50	0.487	8500	3290	38.84%	86	1.02%	39.86%	0.39
BLK3	4.61×10^{-4}	1.74	50	0.487	8500	3290	38.84%	85	1.01%	39.85%	0.28
BLK4	4.61×10^{-4}	1.74	50	0.487	8500	3290	38.84%	85	1.01%	39.85%	0.19
BPK1	4.75×10^{-4}	1.69	50	0.487	8500	3340	39.50%	67	0.79%	40.29%	0.45
BPK2	4.75×10^{-4}	1.69	50	0.487	8500	3340	39.50%	67	0.79%	40.29%	0.4
BPK3	4.75×10^{-4}	1.69	50	0.487	8500	3340	39.50%	66	0.78%	40.29%	0.28
BPK4	4.75×10^{-4}	1.69	50	0.487	8500	3340	39.51%	66	0.78%	40.29%	0.19
BMK1	5.09×10^{-4}	1.58	50	0.487	8500	3120	36.90%	75	0.88%	37.79%	0.44
BMK2	5.09×10^{-4}	1.58	50	0.487	8500	3120	36.90%	75	0.88%	37.79%	0.39
BMK3	5.09×10^{-4}	1.58	50	0.487	8500	3120	36.90%	75	0.88%	37.78%	0.28
BMK4	5.09×10^{-4}	1.58	50	0.487	8500	3120	36.91%	74	0.87%	37.78%	0.18
DSK1	6.42×10^{-4}	1.18	250	0.397	41,200	15,600	37.86%	5410	13.15%	51.01%	0.57
DSK2	6.42×10^{-4}	1.18	250	0.397	41,200	15,600	37.86%	5290	12.85%	50.72%	0.5
DSK3	6.35×10^{-4}	1.18	250	0.397	41,200	15,600	37.86%	5070	12.32%	50.17%	0.39
DSK4	6.35×10^{-4}	1.18	250	0.397	41,200	15,600	37.85%	4720	11.46%	49.31%	0.26
DMK1	7.57×10^{-4}	1.00	250	0.397	41,200	9320	22.64%	4250	10.32%	32.96%	0.57
DMK2	7.57×10^{-4}	1.00	250	0.397	41,200	9320	22.64%	4140	10.06%	32.70%	0.5
DMK3	7.57×10^{-4}	1.00	250	0.397	41,200	9320	22.63%	3910	9.51%	32.14%	0.39
DMK4	7.57×10^{-4}	1.00	250	0.397	41,200	9320	22.63%	3610	8.76%	31.39%	0.26

not depend on the function (linear or power) used to give the fraction of the number concentration of the near-hydrophobic particles, or the average hygroscopicity supposed for all the particles (Fig. 5c).

However, both in the Budapest case (although to a lesser extent) and in the Delhi case (to a larger extent), the efficiency of Brownian scavenging decreases significantly if the hygroscopicity is supposed to be same for all the particles (Fig. 5 and Table 2). These results stem from the fact that if the aerosol particles are identical (BMK1-BMK4 as well as DMK1-DMK4) with respect to hygroscopicity, the width of the wet aerosol/drop spectrum remains smaller during the evolution of the size distribution compared to the other cases (BLK1-BPK4 furthermore DSK1-DSK4). While in the first group of cases the drops can form and grow on both the small aerosols particles (haze) and on the larger ones as well, in the second group of the cases the drops formed on the larger and more water-soluble aerosol particles grow by diffusional growth, and a large fraction of the smaller particles becomes only slightly wet. At 10:30 pm, when the difference between the accumulated Brownian scavenging rates is the largest between the BLK1 and BMK1 cases, the number concentrations of particles smaller than 0.1 μm are 8.48×10^4 and $7.57 \times 10^4 cm^{-3}$, respectively. Furthermore, these numbers in the case of DSK1 and DMK1 at 12:00 am are 1.94×10^6 and 1.47×10^6, respectively. The larger reduction (ca. 25%) of particle concentration in the Delhi case proves that the efficiency of Brownian scavenging is higher if the small aerosol particles (0.1μm) are mostly NH particles (see the initial size distribution of the aerosol particles in Fig. 3). If the aerosol particles are internally mixed, the efficiency of the Brownian scavenging becomes significantly smaller. Fig. 5a reveals that in the Budapest case, the number concentration of captured aerosol particles increases from 8:30 pm to midnight due to the formation and growth of the liquid drops. In the dissipation phase of the fog, the number concentration of captured particles by phoretic forces increases only slightly (Fig. 5a). In the Delhi case the impact of the phoretic scavenging is more significant. This process is efficient at the end of the offset period of the fog (Fig. 5b).

The contour plots in Fig. 6 and Fig. 7 show the time evolution of size distribution of dry aerosol/aerosol inside the droplets over the Budapest and Delhi cases, as well as the size distribution of droplets for the BLK1, BMK1, DSK1 and DMK1 cases. In Fig. 6a and Fig. 7a the solid and dashed lines denote boundaries for the LH and the NH bins, respectively. In Fig. 6b and Fig. 7b the time evolution of the size distribution (DSD) of droplets formed on LH particles is plotted. The solid lines denote the bin boundaries for the liquid drops, both haze and fog drops, in Fig. 6b and d as well in in Fig. 7b and d. The evolution of aerosol size distribution is the consequence of two different processes. The size distribution of NH particles is impacted only by the scavenging processes. The size distribution of the LH particles is also impacted by the scavenging processes, additionally, the broadening of the final bins is the consequence of chemical reactions occurring inside of the water drops (see section 4.3). During the onset period of the fog, the significant decrease of aerosol concentration at the radius smaller than 0.05 μm is the consequence of Brownian scavenging (e.g., Santachiara et al., 2012) both in the Budapest and Delhi case (panels a and c in Fig. 6 and 7). Because of its smaller effect, the impact of phoretic forces cannot be recognized in panels related to the Budapest cases. The efficiency of phoretic scavenging is more obvious in the Delhi case. Fig. 7a and c reveal a significant decrease of the concentration of aerosol particles with a radius around 0.05 μm at the end of the offset period. This difference can be explained by the following two reasons:

- The concentration of aerosol particles at the size of about 0.1 μm is significantly larger in the Delhi case, than in the Budapest case (Fig. 3). At this aerosol size, phoretic scavenging is more dominant than Brownian scavenging, because the Brownian effect is small if the aerosol size is near or larger than 0.1 μm (e.g., Santachiara et al., 2012, 2013).
- During the onset and dissipation periods, aerosol particles with a radius around 0.1 μm can only be captured by water drops due to phoretic forces in a subsaturated environment. The smaller warming rate and the larger hygroscopicity of water-soluble aerosol particles resulted in longer dissipation and subsaturated periods in the Delhi case (Fig. 4).

The contour plots about the drop size distribution both in Fig. 6 and Fig. 7 reveal that the number concentration of droplets larger than the critical radius is small in both Budapest and Delhi case (see also the number concentration of the activated aerosol particles in Table 2). In the mature phase of the fog, drops larger than the critical size keep growing, and they collect the sub-micron particles of the LH and NH modes through Brownian motion. Note, the critical radius is evaluated by using a near constant supersaturation in the mature phase, and not the maximum supersaturation at the end of the onset period. Drops smaller than the critical size evaporate slightly even during the mature phase of the fog (see the time profiles of the bin boundaries for the drops/haze particles). By the end of the dissipation phase of the fog, the drops completely evaporate, and only wet aerosol particles remain.

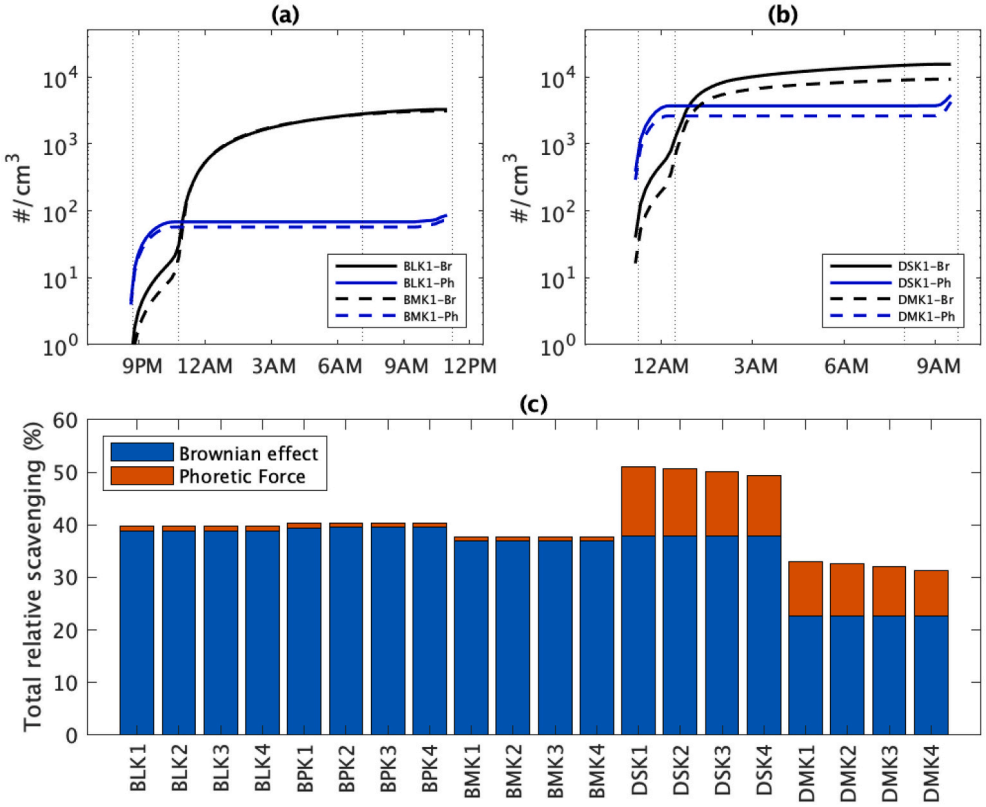

Fig. 5. Cumulative effect of Brownian and phoretic forces on scavenging process in (a): Budapest case and (b): Delhi case. (c): Efficiency of Brownian motion and that of phoretic forces in total scavenging rate. The total relative scavenging means the ratio of the scavenged particle concentration and the total initial aerosol concentration.

Comparison of the size distribution of aerosol particles in the onset and the dissipation period reveals the impact of the scavenging process (see the decrease of the concentration of aerosol particles smaller than 0.1 μm) and the sulphate formation occurring inside of the drops (see the broadening of the aerosol size distribution for particles larger than 0.3 μm in Budapest case and larger than 0.2 μm in Delhi case).

4.3. The impact of liquid chemistry

The initial composition of a droplet is determined by the dissolution of soluble materials contained within an aerosol particle, which serves as the cloud condensation nucleus (CCN). Further variations in the composition come from subsequent scavenging of other non-activated, interstitial particles and from uptake of water-soluble gases and aqueous-phase reactions. We study how the hygroscopicity of the aerosol particles and the concentration of different inorganic trace gases (Table 2) affect the evolution of the chemical characteristics of fog and the aerosol regeneration process. Due to the long lifetime of the fog and the slow sedimentation of the drops, they absorb large amounts of different types of trace gases. All gases are depleted rapidly by drops in line with increases of the LWC (Fig. 8). The amounts of the absorbed gases increase less during the mature phase of the fog, and no further increase occurs during the dissipation period, if LWC decreases significantly.

Fig. 8e and 8f show that the absorption of HNO_3 is affected only by its concentration in the atmosphere. Because the Henry constant of this gas is large, the amount of the absorbed HNO_3 depends neither on the absorption of other gases, nor on the pH of the drops. The absorption of the SO_2 gas is also mostly impacted by the concentration of this gas. However, in the Delhi case, where the concentration of the HNO_3 gas is about 50 times larger than in the Budapest case, the presence of the HNO_3 gas in the atmosphere mitigates the absorption of the SO_2 gas only slightly (see also in Fig. 9). As a result of more pollution (the larger concentration of trace gases and aerosol particles) in the Delhi case, the time profiles describing the absorption of SO_2 and NH_3 diverge during the onset period of the fog. In the Budapest case, due to the less polluted atmosphere, this divergence started a few hours after the onset of the fog. Fig. 8g and 8h show the time profile of the bulk pH and it is calculated by summarizing liquid water content and the different compounds in them over the size spectrum. Comparison of panels c and g, along with panels d and h in Fig. 8 reveals that the absorption of NH_3 is regulated by pH. The pH of the water drops is affected not only by the absorption of the gases previously mentioned, but also the formation of sulfur (VI). The pH of the drops remains in the interval from 5 to 6.5. This enhances the absorption of NH_3 without the drops becoming saturated with respect to the NH_4^+ ions (Schmeller and Geresdi, 2019). As we can see in Fig. 8i and 8j, the time evolution of accumulated $S(VI)$ significantly depends on the amount of SO_2 absorption for both the Budapest and the Delhi cases. In the Delhi case, the uptake of HNO_3 results in the decrease of $S(IV)$ formation by increasing the acidity significantly in fog droplets. Fog becomes the most acidic in the BLK1 and DSK1 cases (HNO_3 is present in the atmosphere and a large amount of SO_2 is absorbed). The lower pH promotes the absorption of NH_3, which results in the enhancement of NH_4^+ ion accumulation (Fig. 9). In the BLK4 and DSK4 cases (a lesser amount of SO_2 is absorbed and the concentration of HNO_3 is set equal to zero) the fog becomes less acidic. The simulated time evolution of pH in the Budapest cases is plotted in Fig. 8g. During the onset period the fog is more acidic (pH = 5.6–5.7) and pH gradually increases with respect to time due to increase of LWC. During the mature period, the pH of the solute concentration remains near constant because the absorption of trace gases and the sulfate formation is balanced by the increase in the drop size. In the dissipation period pH decreases along with LWC mostly due to the evaporation of the droplets. In the more polluted environmental (Delhi case) conditions

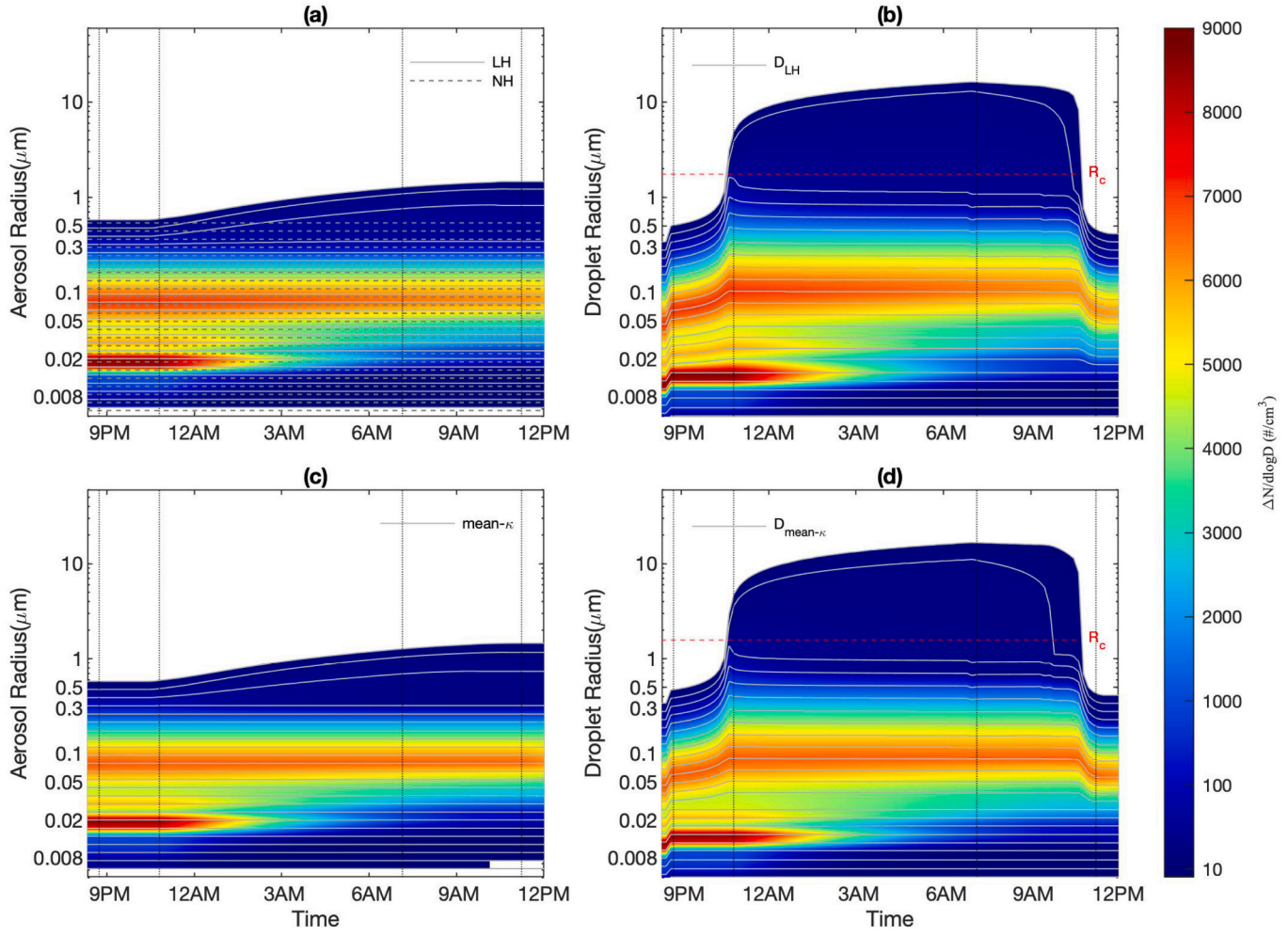

Fig. 6. Contour plots depict the time evolution of aerosol and haze/droplet size distribution for Budapest cases (BLK1 at first row and BMK1 second row). The vertical dotted lines denote the different phases of the fog (see the vertical dashed lines in Fig. 4). R_c means the critical radius for water drops at the supersaturation which occurs during the mature phase of the fog, LH and NH mean less hygroscopic and nearly hydrophobic dry aerosol particles, respectively. Mean-κ means that all dry aerosol particles have the same hygroscopicity, D_{LH} denotes drops formed on LH particles. $D_{mean-\kappa}$ denotes drops formed on aerosol particles having the same hygroscopicity. The time evolution of the bin boundaries for the aerosol particles and liquid drops are depicted as it is given by the fig. legend.

pH reaches nearly 6 at by the end of the onset period, and in the mature period the fog becomes gradually more acidic (Fig. 8h). Because in the Delhi case the LWC remains near constant during the mature phase, the absorption of gases and the sulfate formation results in a decrease of the pH. This decrease becomes more evident in the dissipation phase of the fog. The pH curves are more divergent due to the larger impact of changes in the concentration of gases in Delhi from case to case. Fig. 9 summarizes the results of all chemistry sensitivity tests for the mass concentration of $S(VI)$, NH_4^+, NO_3^- formed and accumulated inside of the droplets by the end of fog dissipation phase. The pattern of the histograms reveals that size dependence of the hygroscopicity has no effect on the liquid chemistry occurring in the drops. Our model results also show that $S(VI)$ has significant role, and it modulates the fog acidity over both Budapest and Delhi (Fig. 8i and 8j). Fig. 9 shows that large amounts of $S(VI)$ correspond highly to the amount of total $SO_2(g)$ absorption. As expected, the mass concentration of NH_4^+ depends on the absorption of $SO_2(g)$ and on the absence/presence of $HNO_3(g)$. The amount of the mass concentration of $S(VI)$ is also affected (slightly reduction) by the presence of $HNO_3(g)$. The final column in Table 2 gives the broadening of the size distribution of aerosol particles due to the liquid chemistry. In Fig. 6a, 6c and Fig. 7a, 7c the time profiles of solid grey lines depicting the evolution of the size distribution of aerosol particles reveal the broadening of the distribution due to the liquid chemistry. The mass of aerosol particles is increased by the accumulated ions of $S(VI)$, NH_4^+, NO_3^-. The addition of these species not only increases the mass of the aerosol particles, but they change the hygroscopicity of the particles as well. The impact of the collected hydrophobic particles is negligible because their mass is about one – two orders of magnitude less than the mass of the sulfate formed inside of the drops. Fig. 10 shows the calculated new hygroscopicity parameter for each bin for the regenerated aerosol particles at the end of the dissipation phase for all sensitivity tests. The new hygroscopicity parameter is calculated by the volume weighted averages by following equation (Petters and Kreidenweis, 2007):

$$\kappa_i = \frac{V_{i,o}\kappa_{LH} + V_{i,s}\kappa_s}{V_{i,o} + V_{i,s}} \tag{4}$$

where $V_{i,\,o}$ and $V_{i,\,s}$ are the volumes of the less hygroscopic particles and those of the sulphate forms in the i^{th} bin, respectively. κ_{LH3pt} and κ_s are the hygroscopicity parameters for the less-hygroscopicity particles, and for the sulphate compounds. We suppose that the hygroscopicity of the mix of NH_4^+, NO_3^- and $S(VI)$ ions is 0.6 (Note: liquid chemistry was simulated for the drops with radius of equal or larger than 1 μm).

The hygroscopicity related to the smallest sizes was not impacted by the chemistry (see the size limit for the liquid chemistry above), so these values are equal to the initial ones. The sensitivity test reveals that initial

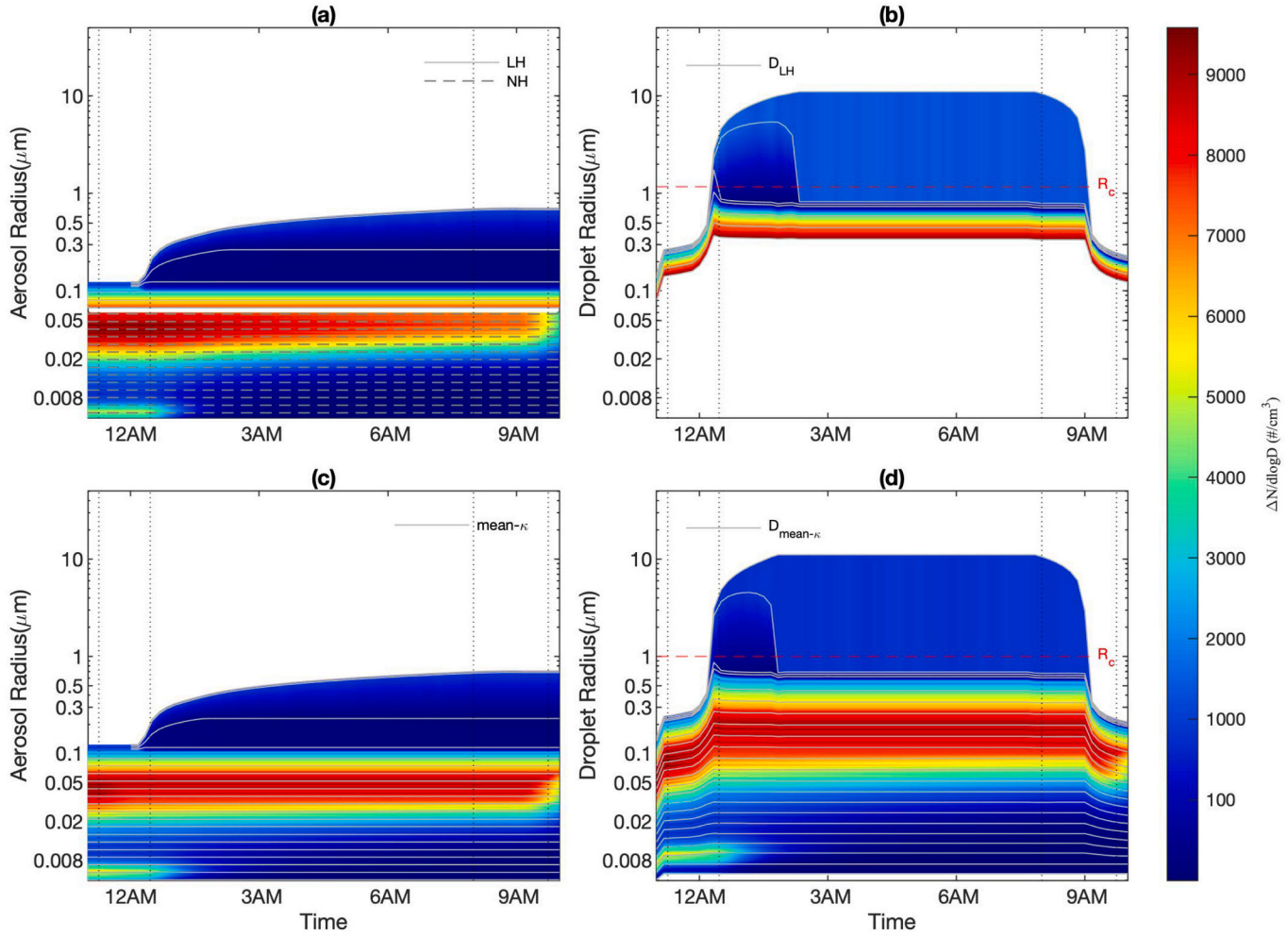

Fig. 7. Contour plots depict the time evolution of aerosol and haze/droplet size distribution for Delhi cases (DSK1 at first row and DMK1 second row). The vertical dotted lines denote the different phases of the fog (see the vertical dashed lines in Fig. 4). R_c means the critical radius for water drops at the supersaturation which occurs during the mature phase of the fog, LH and NH mean less hygroscopic and nearly hydrophobic dry aerosol particles, respectively. Mean-κ means that all dry aerosol particles have the same hygroscopicity, D_{LH} denotes drops formed on LH particles. $D_{mean-\kappa}$ denotes drops formed on aerosol particles having the same hygroscopicity. The time evolution of the bin boundaries for the aerosol particles and liquid drops are depicted as it is given by the fig. legend.

conditions for the size dependence of the hygroscopicity has no effect on the hygroscopicity of the regenerated aerosol particles with a radius larger than 0.3 μm in neither the Budapest nor in Delhi cases. This finding stems from the fact that the chemical processes occurring in the liquid drops formed on LH aerosol particles do not depend on the value of hygroscopicity. In the Budapest case the final hygroscopicity depends on the initial concentration of the trace gases. While in BLK1 and BLK2 cases the hygroscopicity increases to nearly 0.6 for the radius larger than 0.3 μm due to a large amount of SO_2 and the presence of HNO_3 in the BLK1 case, meanwhile in the BLK4 cases the hygroscopicity increases only to 0.5. In the Delhi case, the hygroscopicity of the regenerated aerosol particles do not vary from case to case due to the high amount of trace gas concentration available in the environment in each investigated case.

5. Discussion

A detailed, bin scheme was developed to simulate the life cycle of the fog. The impact of neglecting the dynamic and radiation processes were lessened by tracking the simulated time profile of the temperature with the observed time profile. The simulated life cycle of fog is in line with the observed life cycle in the Budapest case, while a slight bias occurs in the Delhi case. The simplified fog dynamic allows us to focus on the different types of scavenging processes, and tracking the evolution of the drop size distribution formed on both activated and interstitial aerosol particles (haze particles). To the extent of the knowledge of the authors, a bin scheme has been never implemented in a numerical model for the simulation of liquid chemistry in fog.

The role of the scavenging processes in clouds has been published in many papers (e.g., Flossmann et al., 1985). While in the clouds, the activation significantly reduces the number concentration of the hygroscopic particles and the scavenging processes play a less important role (Geresdi et al., 2005), due to the very small value of supersaturation, the activation (Table 2) has a very small role in reducing the number concentration of hygroscopic aerosol particles in the fog. However, a self-cleaning (scavenging) process explained through Brownian motion and phoretic force in fog (Fig. 5) significantly reduces the number concentration of the aerosol particles with a radius less than 0.1 μm (Fig. 6 and 7). Although the rate of the Brownian and phoretic scavenging is small, they can have significant impact due to the long lifetime of the fog. The number concentration of activated aerosol particles is about one order of magnitude less than the decrease of the number concentration due to Brownian and phoretic scavenging. Note, the hygroscopicity of the LH particles is less than 0.5 (Table 2) in our simulated cases. The role of activation scavenging can be more important if the hygroscopicity of the aerosol particles is significantly larger

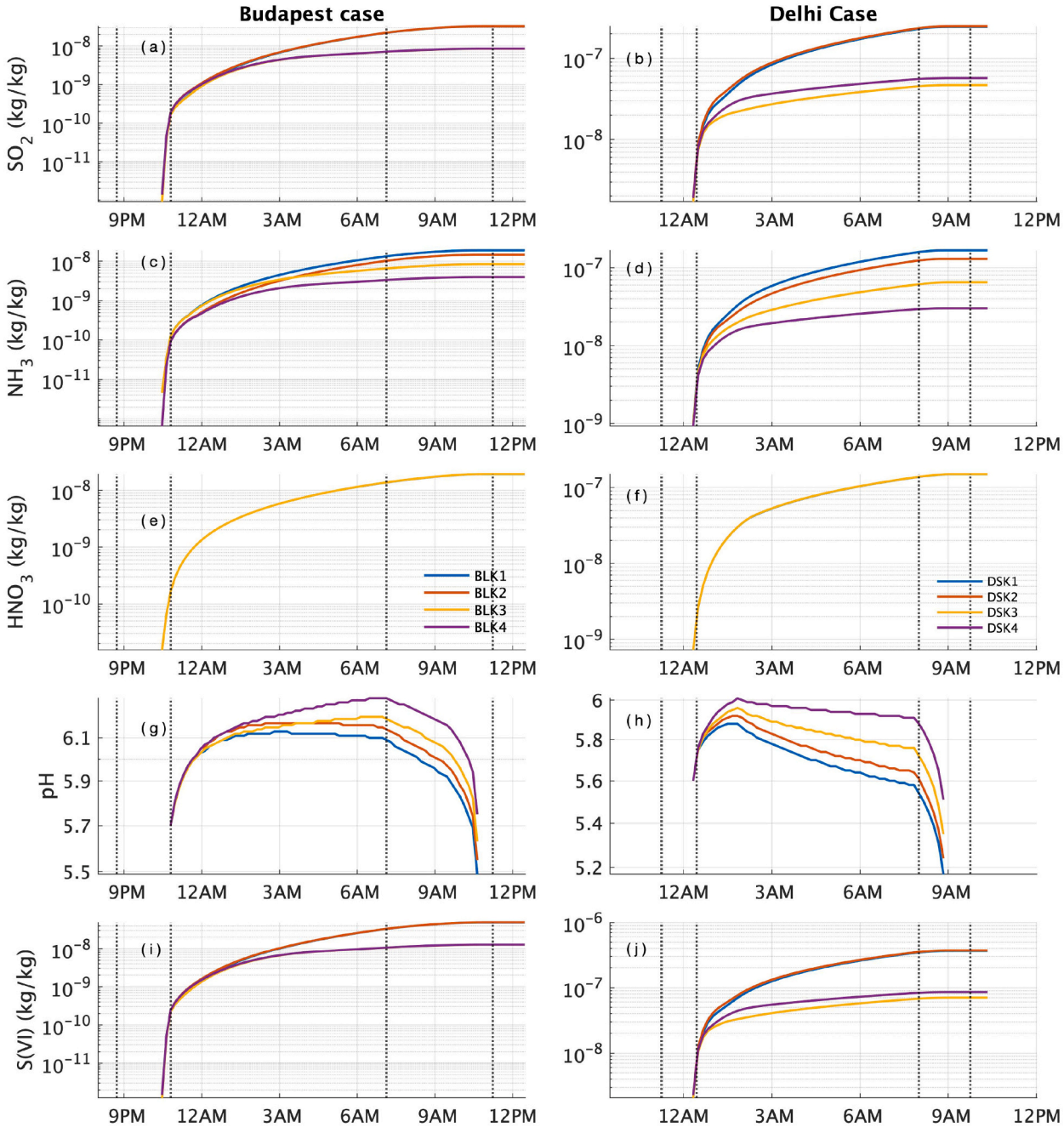

Fig. 8. Time evolution of the accumulated absorption of trace gases (panels (a) – (f)), bulk pH (panels (g) and (h)) and accumulated S(VI) (panels (i) and (j)). The different lines with different colors denote different cases (see the legends in panels (e) and (f)).

than in our case studies (Gilardoni et al., 2014). On the basis of their field observation performed in Indo Gangetic Plain, Izhar et al., 2020 also concluded that the scavenging processes significantly reduce the amount of the aerosol in fog. The results of our study suggest that the initial size dependence of the hygroscopicity of aerosol particles can have a significant effect on the efficiency of Brownian scavenging. Unfortunately, the size dependence of the hygroscopicity is not available from most of the field observations. However, some field experiment suggest that aerosol particles with a radius smaller than 100 nm are mostly hydrophobic (e.g., Wang et al., 2018; Enroth et al., 2018). Our results show that these small aerosol particles are efficiently collected by the fog droplets due to the long lifetime of the fog. The role of the phoretic forces in the impaction scavenging is controversial. Geresdi et al., 2005 asserted that phoretic force has no significant impact in stratified clouds when compared to activation. However, our sensitivity test reveals that the efficiency of phoretic scavenging can be more decisive, and its role in reducing the concentration of aerosol particles with a radius about 0.1 μm depends on the duration of the onset and dissipation periods of the fog.

The dashed lines in Fig. 1e and 1f reveal the simulated time profiles of the particle concentration (aerosol particles as well as both haze particles and droplets are considered). Due to the applied observational technique, these plots show not only the interstitial aerosol particles but include aerosol particles inside the water drops (activated aerosol particles). As such, the sedimentation of fog drops and the impaction scavenging should have resulted in the observed decrease of the aerosol particle concentration. Although in our model the local emission and the advection of the particles, as well as the sedimentation of the fog drops

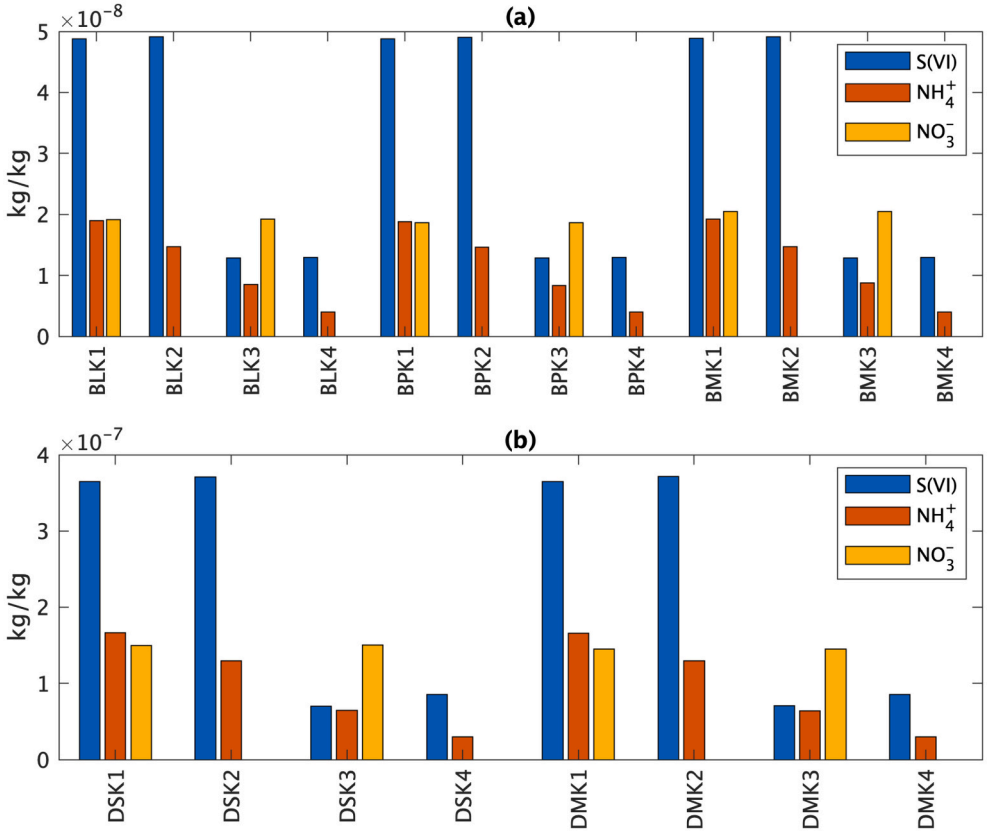

Fig. 9. Mass concentration of $S(VI)$, NH_4^+, NO_3^- for the sum of the regenerated aerosol particles by the end of the dissipation phase for Budapest (a) and Delhi (b).

are not taken into consideration in the Budapest case, the time profile of the simulated concentration is in line with the observation data which is to say that the decrease of the particle concentration in the Budapest case can be explained by the scavenging processes. In the Delhi case, the difference between the simulated and observed profiles is significant. This difference between the two cases may stem from the fact that while in downtown Budapest the emission rate due to local sources (vehicle traffic) must have been small during the night, in the Delhi case the local emission due to the exhaust of airplanes is significant even during the night (see spikes in the observed time profile of the particle concentration in Fig. 1f).

The advantages of using bin resolved liquid chemistry against the bulk chemistry was published by Schmeller and Geresdi, 2019. Due to the size resolved simulation of the liquid chemistry the model output allows to reveal both the size dependence of the pH of the fog drops and the bulk pH. Because during the field projects the size resolved pH values are not available, the time profiles of the bulk pH are plotted in Fig. 8g and h. The lower pH in the Delhi case compared to the Budapest case is in line with results published by Wang et al., 2020. They asserted that fog formed in less polluted air mass had much higher pH than polluted haze under high ammonia (NH_3) conditions. Ghude et al., 2017 showed the fog water pH varied between 6.12 and 7.62 with an average of 6.91, which indicates the alkaline nature over Delhi. Also, Nath and Yadav, 2018 published results about analyzing the chemical compounds in fog and dew samples collected during the winter of 2014–2015 over Delhi (7 km distance from WIFEX site) and reported the mean bulk ion concentrations inside the drops and bulk pH of the droplets. Nath and Yadav, 2018 found that the pH of the droplets is more acidic, and it changes between 4.0 and 6.6, and that the ratio of the masses of the two acidic compounds of $S(VI)$ and NO_3^- was about two. Comparing this observed data with our simulated results is not evident, because data about trace gas concentrations was not published in Nath and Yadav, 2018. However, the ratio of the masses of the two acidic compounds ($S(VI)/NO_3^-$) and the calculated pH of the fog drops for the DSK1and DMK1 cases (Fig. 8h and Fig. 9) is in line with the observations of Nath and Yadav, 2018. However, our results also shows that the pH of the drops can change in wide intervals during the evolution of the fog in highly polluted atmospheres even in the mature period. As such, the measured pH may depend on the timing of the sampling.

The importance of the fog - aerosol interaction has been presented in a number of papers (e.g., Boutle et al., 2018). These studies have mostly focused on the microphysical processes, and less attention has been devoted to the aging of the aerosol particles due to liquid chemistry in fog (e.g., Izhar et al., 2020). The bin resolved liquid chemistry model allows us to track the changes in the chemical composition of each bin. Due to liquid chemistry in fog droplets, both the chemical composition and the mass of the aerosol particles are subject to change Fig. 6a, 6c and Fig. 7a, 7c, show the aerosol size distribution along with time and the broadening of the spectrum (mostly at larger particles) for both the Budapest and the Delhi case. These regenerated aerosols contain ionic compounds which formed through the liquid chemistry and have more hygroscopicity due to their ionic nature. This result of our numerical experiment is in line with the findings of a field experiment published by Izhar et al., 2020. They asserted, that the enhancement of sulfate concentration in fog water was due to the liquid chemistry, which results in an increase of the aerosol mass after the evaporation of fog droplets. The enhancement of the hygroscopicity (Fig. 10) can impact the evolution of the fog as follows: (i) The dissipation of the fog can be mitigated by the enhanced solution effect. (ii) The increased solubility of the regenerated aerosol particles can assist the formation of the successive fog formation. In this study the simulation of liquid chemistry is confined to the drops larger than 1 μm. Because supersaturation is small in the fog, the initial size of the aerosol particles inside these drops is larger than 0.1 μm. As such, we cannot follow the impact of the liquid chemistry in the case aerosol particles smaller than 0.1 μm, and we cannot deduce how the liquid chemistry impacts the size dependence of the hygroscopicity of

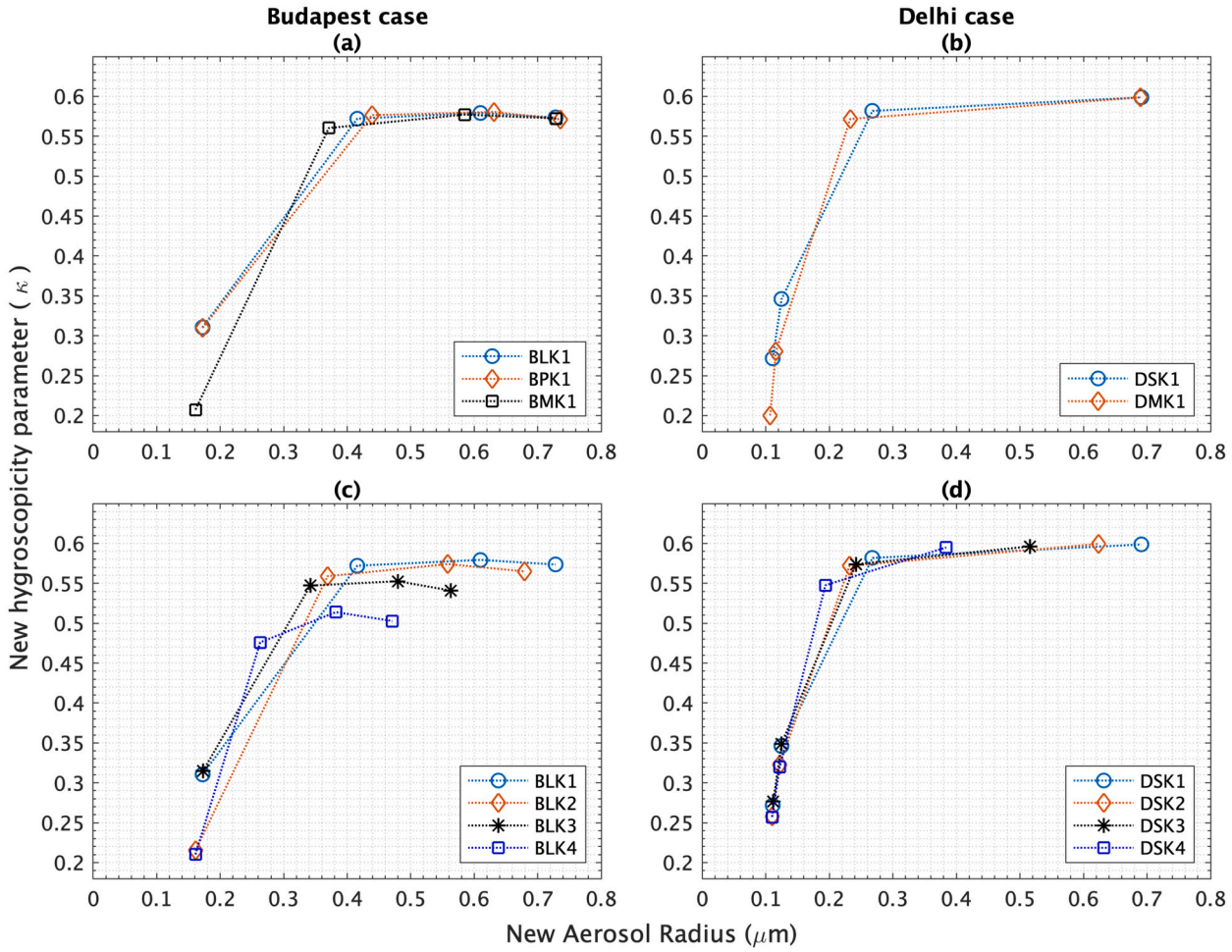

Fig. 10. New hygroscopicity parameter for the regenerated aerosol particles at end of fog for the Budapest and Delhi cases.

these small aerosol particles. We can conclude that due to the long residence time of the droplets in the fog, the liquid chemistry has an impact on the hygroscopicity of the regenerated aerosol particles, and in a more polluted atmosphere the hygroscopicity becomes larger than in a less polluted atmosphere.

6. Conclusions

The interaction between fog microphysics and liquid chemistry was examined with a box model for two distinctive locations of Budapest, Hungary and Delhi, India. This model involves a detailed moving bin microphysics scheme to properly simulate the diffusional growth and evaporation of water drops, as well as the liquid chemistry. A comprehensive sensitivity study has been carried out to investigate how the initial hygroscopicity of aerosol impacts the scavenging of sub-micron particles through different mechanisms, and liquid chemistry. Also, the impact of atmospheric pollution characterised by the concentration of SO_2, H_2O_2, O_3, HNO_3, CO_2 and NH_3 gases on $S(VI)$, NH_4^+, NO_3^- accumulating inside of water drops is studied. On the base of the results of the numerical simulations the conclusions are as follows:

- Due to the low supersaturation, particle scavenging through activation nucleation is less important than other mechanisms, such as Brownian and phoretic. On an average, 40–50% total particles are collected due to impact scavenging (Fig. 5), and less than 1% of the LH particles are activated due to the low supersaturation and small hygroscopicity of the LH particles.
- The role of phoretic scavenging depends on the concentration of aerosol particles with a radius around 0.1 μm, as well as on the duration of the dissipation phase of the fog.
- Due to the long duration of the fog, the droplets absorb significant amounts of different trace gases. Since the presence and absorption of ammonia promote the absorption of SO_2 the sulfate formation is very efficient in the simulated cases.
- The acidity of the drops is affected not only by the liquid chemistry, but it also depends on the diffusional growth of the drops. While the increase of the LWC results in the increase of the bulk pH, the evaporation of the drops in the dissipation periods significantly reduces the pH.
- Our numerical model allows us to track the accumulation of chemical compounds such as $S(VI)$, NH_4^+, NO_3^- inside of the drops. Additionally it should be noted that the size dependence of hygroscopicity has no effect on the liquid chemistry occurring in the drops.
- The results reveal that liquid chemistry contributes to the broadening of the aerosol size distribution (regenerated aerosol or aging of the aerosol), and significantly increases the hygroscopicity of the regenerated aerosol particles formed after the evaporation of the liquid phase. This increased hygroscopicity may impact the duration of fog dissipation by enhancing the solution effect and helps to promote successive fog event in favorable environmental conditions.

The current research raises the following questions, which we intend to solve in the next phase of the research: (i) The evaluation of the impact of liquid chemistry on hygroscopicity in a wider range of the size of the aerosol particles require the extension of the numerical simulation

of the chemistry for the droplets smaller than 1 Âµm. (ii) The enhancement of hygroscopicity of aerosol particles on the subsequent formation of fog is planned to be simulated. Furthermore, the effect of organic compounds is also planned to be studied by taking into consideration the absorption of trace gases such as formaldehyde or acetic acid.

Declaration of Competing Interest

None.

Acknowledgement

This research was supported by the GINOP-2.3.2-15-2016-00055 project, financed by the Ministry of Finance and by the Hungarian Scientific Research Fund (K132254).

References

Acharja, P., Ali, K., Trivedi, D.K., Safai, P.D., Ghude, S., Prabhakaran, T., Rajeevan, M., 2020. Characterization of atmospheric trace gases and water soluble inorganic chemical ions of PM1 and PM2.5 at Indira Gandhi International Airport, New Delhi during 2017-18 winter. Sci. Total Environ. 729, 138800. URL. https://doi.org/10.1016/j.scitotenv.2020.138800.

Arub, Z., Bhandari, S., Gani, S., Apte, J.S., Hildebrandt Ruiz, L., Habib, G., 2020. Air mass physiochemical characteristics over New Delhi: impacts on aerosol hygroscopicity and cloud condensation nuclei (CCN) formation. Atmos. Chem. Phys. 20, 6953–6971. https://doi.org/10.5194/acp-20-6953-2020.

Bott, A., Sievers, U., Zdunkowski, W., 1990. A Radiation Fog Model with a Detailed Treatment of the Interaction between Radiative Transfer and Fog Microphysics. URL http://journals.ametsoc.org/doi/abs/10.1175/1520-0469%281990%29047%3C2153%3AARFMWA%3E2.0.CO%3B2. https://doi.org/10.1175/1520-0469(1990)047<2153:ARFMWA>2.0.CO;2.

Boutle, I., Price, J., Kudzotsa, I., Kokkola, H., Romakkaniemi, S., 2018. Aerosol-fog interaction and the transition to well-mixed radiation fog. Atmos. Chem. Phys. 18, 7827–7840. https://doi.org/10.5194/acp-18-7827-2018.

Chaouch, N., Temimi, M., Weston, M., Ghedira, H., 2017. Sensitivity of the meteorological model WRF-ARW to planetary boundary layer schemes during fog conditions in a coastal arid region. Atmos. Res. 187, 106–127. URL. https://doi.org/10.1016/j.atmosres.2016.12.009.

Cui, C., Bao, Y., Yuan, C., Li, Z., Zong, C., 2019. Comparison of the performances between the WRF and WRF-LES models in radiation fog – a case study. Atmos. Res. 226, 76–86. URL. https://doi.org/10.1016/j.atmosres.2019.04.003.

Elbert, W., Hoffmann, M.R., Krämer, M., Schmitt, G., Andreae, M.O., 2000. Control of solute concentrations in cloud and fog water by liquid water content. Atmos. Environ. 34, 1109–1122.

Enroth, J., Mikkilä, J., Németh, Z., Kulmala, M., Salma, I., 2018. Wintertime hygroscopicity and volatility of ambient urban aerosol particles. Atmos. Chem. Phys. 18, 4533–4548. https://doi.org/10.5194/acp-18-4533-2018.

Flossmann, A.I., Hall, W.D., Pruppacher, H.R., 1985. A theoretical study of the wet removal of atmospheric pollutants. part i: the redistribution of aerosol particles captured through nucleation and impaction scavenging by growing cloud drops. J. Atmos. Sci. 42, 583–606, 10.1175/1520-0469(1985)042<0583:ATSOTW>2.0.CO;2 URL: https://journals.ametsoc.org/view/journals/atsc/42/6/1520-0469_1985_042_0583_atsotw_2_0_co_2.xml.

Geresdi, I., Rasmussen, R., 2005. Freezing drizzle formation in stably stratified layer clouds. Part II: the role of giant nuclei and aerosol particle size distribution and solubility. J. Atmos. Sci. 62, 2037–2057. https://doi.org/10.1175/JAS3452.1.

Geresdi, I., Rasmussen, R., Grabowski, W., Bernstein, B., 2005. Sensitivity of freezing drizzle formation in stably stratified clouds to ice processes. Meteorog. Atmos. Phys. 88, 91–105. https://doi.org/10.1007/s00703-003-0048-5.

Ghude, S.D., Bhat, G.S., Prabhakaran, T., Jenamani, R.K., Chate, D.M., Safai, P.D., Karipot, A.K., Konwar, M., Pithani, P., Sinha, V., Rao, P.S., Dixit, S.A., Tiwari, S., Todekar, K., Varpe, S., Srivastava, A.K., Bisht, D.S., Murugavel, P., Ali, K., Mina, U., Dharua, M., Jaya Rao, Y., Padmakumari, B., Hazra, A., Nigam, N., Shende, U., Lal, D. M., Chandra, B.P., Mishra, A.K., Kumar, A., Hakkim, H., Pawar, H., Acharja, P., Kulkarni, R., Subharthi, C., Balaji, B., Varghese, M., Bera, S., Rajeevan, M., 2017. Winter fog experiment over the Indo-Gangetic plains of India. Curr. Sci. 112, 767–784. https://doi.org/10.18520/cs/v112/i04/767-784.

Gilardoni, S., Massoli, P., Giulianelli, L., Rinaldi, M., Paglione, M., Pollini, F., Lanconelli, C., Poluzzi, V., Carbone, S., Hillamo, R., Facchini, M., Fuzzi, S., 2014. Fog scavenging of organic and inorganic aerosol in the po valley. Atmos. Chem. Phys. 14, 6967–6981. https://doi.org/10.5194/acp-14-6967-2014.

Gultepe, I., 2019. Low-Level Ice Clouds-Ice Fog. Encylopedia of Water: Science, Technology, and Society, pp. 1–19. URL. https://doi.org/10.1002/9781119300762.wsts0140.

Gultepe, I., Müller, M.D., Boybeyi, Z., 2006. A new visibility parameterization for warm-fog applications in numerical weather prediction models. J. Appl. Meteorol. Climatol. 45, 1469–1480. https://doi.org/10.1175/JAM2423.1.

Gultepe, I., Pagowski, M., Reid, J., 2007a. A satellite-based fog detection scheme using screen air temperature. Weather Forecast. 22, 444–456. https://doi.org/10.1175/WAF1011.1.

Gultepe, I., Tardif, R., Michaelides, S.C., Cermak, J., Bott, A., Bendix, J., Müller, M.D., Pagowski, M., Hansen, B., Ellrod, G., Jacobs, W., Toth, G., Cober, S.G., 2007b. Fog Research: A Review of Past Achievements and Future Perspectives. https://doi.org/10.1007/s00024-007-0211-x.

Izhar, S., Gupta, T., Panday, A.K., 2020. Scavenging efficiency of water soluble inorganic and organic aerosols by fog droplets in the Indo Gangetic Plain. Atmos. Res. 235, 104767. URL. https://doi.org/10.1016/j.atmosres.2019.104767.

Kerminen, V.M., Wexler, A.S., 1995. Growth laws for atmospheric aerosol particles: an examination of the bimodality of the accumulation mode. Atmos. Environ. 29, 3263–3275. https://doi.org/10.1016/1352-2310(95)00249-X.

Kunkel, B.A., 1982. Microphysical properties of fog at Otis AFB. Environ. Res. Papers 113.

Mazoyer, M., Burnet, F., Denjean, C., Roberts, G.C., Dupont, J.C., Elias, T., 2019. Experimental study of the aerosol impact on fog microphysics at the Instrumented Site for Atmospheric Remote Sensing. Atmos. Chem. Phys. 19, 4323–4344. URL. https://doi.org/10.5194/acp-19-4323-2019.

Meng, Z., Seinfeld, J.H., 1994. On the source of the submicrometer droplet mode of urban and regional aerosols. Aerosol Sci. Technol. 20, 253–265. https://doi.org/10.1080/02786829408959681.

Nath, S., Yadav, S., 2018. A comparative study on fog and dew water chemistry at New Delhi, India. Aerosol Air Qual. Res. 18, 26–36. https://doi.org/10.4209/aaqr.2017.01.0033.

Petters, M.D., Kreidenweis, S.M., 2007. A single parameter representation of hygroscopic growth and cloud condensation nucleus activity. Atmos. Chem. Phys. Discuss. 6, 8435–8456. https://doi.org/10.5194/acpd-6-8435-2006.

Pithani, P., Ghude, S.D., Jenamani, R.K., Biswas, M., Naidu, C.V., Debnath, S., Kulkarni, R., Dhangar, N.G., Jena, C., Hazra, A., Phani, R., Mukhopadhyay, P., Prabhakaran, T., Nanjundiah, R.S., Rajeevan, M., 2020. Real-time forecast of dense fog events over delhi: the performance of the WRF Model during the WiFEX Field Campaign. Weather Forecast. 35, 739–756. https://doi.org/10.1175/waf-d-19-0104.1.

Pringle, K.J., Tost, H., Pozzer, A., Pöschl, U., Lelieveld, J., 2010. Global distribution of the effective aerosol hygroscopicity parameter for CCN activation. Atmos. Chem. Phys. 10, 5241–5255. https://doi.org/10.5194/acp-10-5241-2010.

Pruppacher, H., Klett, J., 2010. Microphysics of clouds and precipitation. In: Volume 18 of *Atmospheric and Oceanographic Sciences Library*, 2 ed. Springer Netherlands, Dordrecht. https://doi.org/10.1007/978-0-306-48100-0. URL.

Salma, I., Németh, Z., Kerminen, V.M., Aalto, P., Nieminen, T., Weidinger, T., Molnár, Á., Imre, K., Kulmala, M., 2016. Regional effect on urban atmospheric nucleation. Atmos. Chem. Phys. 16, 8715–8728. https://doi.org/10.5194/acp-16-8715-2016.

Santachiara, G., Prodi, F., Belosi, F., 2012. A Review of Termo- and Diffusio-Phoresis in the Atmospheric Aerosol Scavenging Process. Part 1 : Drop Scavenging, 2012, pp. 148–158.

Santachiara, G., Prodi, F., Belosi, F., 2013. Atmospheric aerosol scavenging processes and the role of thermo- and diffusio-phoretic forces. Atmos. Res. 128, 46–56. URL. https://doi.org/10.1016/j.atmosres.2013.03.004.

Schmeller, G., Geresdi, I., 2019. Study of interaction between cloud microphysics and chemistry using coupled bin microphysics and bin aqueous chemistry scheme. Atmos. Environ. 198, 366–380. URL. https://doi.org/10.1016/j.atmosenv.2018.10.064.

Silverman, B.A., Weinstein, A.I., Hess, W., 1974. Fog. In: Weather and Climate Modification.

Song, J.I., Yum, S.S., Gultepe, I., Chang, K.H., Kim, B.G., 2019. Development of a new visibility parameterization based on the measurement of fog microphysics at a mountain site in Korea. Atmos. Res. 229, 115–126. URL. https://doi.org/10.1016/j.atmosres.2019.06.011.

Steinfeld, J.I., 1998. Atmospheric chemistry and physics: from air pollution to climate change. Environ. Sci. Policy Sustain. Dev. 40, 26.

Wang, X., Ye, X., Chen, H., Chen, J., Yang, X., Gross, D.S., 2014. Online hygroscopicity and chemical measurement of urban aerosol in Shanghai, China. Atmos. Environ. 95, 318–326. URL. https://doi.org/10.1016/j.atmosenv.2014.06.051.

Wang, X., Shen, X.J., Sun, J.Y., Zhang, X.Y., Wang, Y.Q., Zhang, Y.M., Wang, P., Xia, C., Qi, X.F., Zhong, J.T., 2018. Size-resolved hygroscopic behavior of atmospheric aerosols during heavy aerosol pollution episodes in Beijing in December 2016. Atmos. Environ. 194, 188–197. https://doi.org/10.1016/j.atmosenv.2018.09.041.

Wang, J., Li, J., Ye, J., Zhao, J., Wu, Y., Hu, J., Liu, D., Nie, D., Shen, F., Huang, X., Huang, D.D., Ji, D., Sun, X., Xu, W., Guo, J., Song, S., Qin, Y., Liu, P., Turner, J.R., Lee, H.C., Hwang, S., Liao, H., Martin, S.T., Zhang, Q., Chen, M., Sun, Y., Ge, X., Jacob, D.J., 2020. Fast sulfate formation from oxidation of SO2 by NO2 and HONO observed in Beijing haze. Nat. Commun. 11, 1–7. URL. https://doi.org/10.1038/s41467-020-16683-x.

Xue, J., Yu, X., Yuan, Z., Griffith, S.M., Lau, A.K., Seinfeld, J.H., Yu, J.Z., 2019. Efficient control of atmospheric sulfate production based on three formation regimes. Nat. Geosci. 12, 977–982. URL. https://doi.org/10.1038/s41561-019-0485-5.